Adiabatic passage through chaos

Amit Dey[1], Doron Cohen[2], Amichay Vardi[1]
[1] *Department of Chemistry, Ben-Gurion University of the Negev, Beer-Sheva 84105, Israel*
[2] *Department of Physics, Ben-Gurion University of the Negev, Beer-Sheva 84105, Israel*

We study the process of nonlinear stimulated Raman adiabatic passage within a classical mean-field framework. Contrary to the prevailing dogma, the breakdown of adiabaticity in the interacting non-integrable system, is not related to bifurcations in the energy landscape, but rather to the emergence of quasi-stochastic motion that drains the followed quasi-stationary state. Consequently, faster sweep rate, rather than quasi-static variation of parameters, is better for adiabaticity.

Adiabatic passage is a major tool of quantum control and quantum state engineering. For two-level systems, the Landau-Zener-Stuckelberg-Majorana linear crossing [1–4] has been a prominent paradigm. Three level configurations offer, in addition to Landau-Zener-like rapid adiabatic passage (RAP) schemes, also the possibility of stimulated Raman adiabatic passage (STIRAP) [5, 6] in which an interference-induced dark state supports the efficient transfer of population from source to target state without projection onto an intermediate (often spontaneously decaying) state.

Advances in the field of Bose-Einstein condensation (BEC) have triggered great interest in the application of adiabatic passage to many-body interacting systems. Two-mode adiabatic schemes were modelled by the Bose-Hubbard dimer Hamiltonian, using either classical nonlinear mean-field theory [7–13] or quantum many-body methods [11, 14–19]. Transfer efficiency was found to have a power-law dependence on the sweep rate, with an unavoidable nonadiabatic fraction beyond a critical interaction strength. Similar results were obtained for coupled atomic and molecular condensates [20–28]. The common denominator for all these studies is the quest for energetic stability: *Nonlinear instability is attributed to the emergence of a separatrix in the energy landscape.*

The same energetic stability paradigm was adopted for adiabatic passage in the three-mode trimer [30–34]: The stationary points (SPs) of the energy landscape were found as a function of time, resulting in a bifurcation diagram that reflects topological changes in the energy landscape. Such bifurcations, notably the 'horn' avoided crossing in the nonlinear STIRAP case [30], were assumed to cause the breakdown of adiabaticity. However the three-mode system offers richer physics due to its inherent nonintegrability. Specifically, *dynamical stability* should be distinguished from *energetic stability*, and different dynamical domains can coexist on the same energy surface [29]. The bifurcation diagram lacks essential information on this mixed chaotic phasespace structure.

Outline.– We show that the adiabatic passage efficiency is drastically affected by the *appearance of chaotic regions, whose existence is not related to the SP bifurcation diagram.* Consequently the analysis of adiabatic passage goes beyond the prevailing energetic stability paradigm. Specifically, reduced efficiency in STIRAP is observed even in the absence of avoided crossings. We establish that the breakdown of adiabaticity occurs during specific time intervals in which the followed-SP becomes immersed in chaotic strips on the *same* energy surface. One outcome of this novel breakdown mechanism, is that adiabaticity may be restored by *faster* variation of the control parameter, so as to guarantee that the chaotic interval is traversed before ergodization takes place.

STIRAP.– Many-body STIRAP is modelled by the time-dependent Bose-Hubbard trimer Hamiltonian [30, 35–42] for N particles in three second-quantized modes:

$$\mathcal{H} = \mathcal{E}\hat{n}_2 + \frac{U}{2}\sum_{j=1}^{3}\hat{n}_i^2 - \frac{1}{2}\left(\Omega_p(x)\hat{a}_2^\dagger\hat{a}_1 + \Omega_s(x)\hat{a}_3^\dagger\hat{a}_2 + h.c.\right) \quad (1)$$

Here, $\hat{a}_j$, $\hat{a}_j^\dagger$ are boson annihilation and creation operators with associated occupation operators $\hat{n}_j \equiv \hat{a}_j^\dagger\hat{a}_j$. The interatomic interaction is U, while $\mathcal{E}$ is equivalent to the one-photon detuning of the optical scheme [5, 6]. In STIRAP, the couplings are Gaussian Stokes and Pump pulses $\Omega_{s,p}(x) = Ke^{-(x-x_{s,p})^2}$ which depend on the dimensionless parameter x. The standard realization is a simple constant-rate sweep $x(t) = t/\tau$, with a 'counter-intuitive' sequence $t_p - t_s = (x_p - x_s)\tau > 0$ (see Fig.1a). The system is prepared in the first mode ($n_1(0) = N$). For $U = 0$, an adiabatic sweep transfers the population to the third mode ($n_3(\infty) = N$) by following a coherent dark eigenstate that does not project on the intermediate mode at any time ($n_2(t) = 0$). The studied effect is the breakdown of this adiabatic 100% efficiency in the presence of repulsive interactions ($U > 0$).

Classical dynamics.– In classical mean-field theory, field operators are replaced by c-numbers $\hat{a}_j \mapsto a_j \equiv \sqrt{n_j}e^{i\phi_j}$. Rescaling $a_j \mapsto a_j/\sqrt{N}$, and $t \mapsto Kt$, we obtain the nonlinear Schrödinger equations [30]:

$$i\begin{pmatrix}\dot{a}_1\\ \dot{a}_2\\ \dot{a}_3\end{pmatrix} = \begin{pmatrix} u\,|a_1|^2 & -\frac{g_p}{2} & 0\\ -\frac{g_p}{2} & \varepsilon + u\,|a_2|^2 & -\frac{g_s}{2}\\ 0 & -\frac{g_s}{2} & u\,|a_3|^2\end{pmatrix}\begin{pmatrix}a_1\\ a_2\\ a_3\end{pmatrix} \quad (2)$$

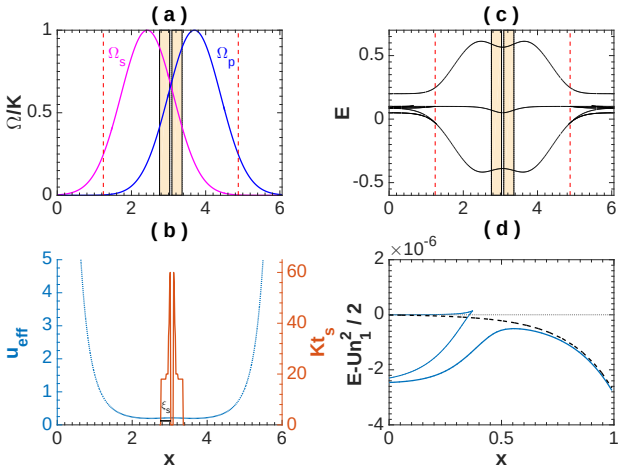

FIG. 1. (color online) **(a)** The STIRAP counter-intuitive pulse scheme. Here and throughout the manuscript, the shaded intervals correspond to the range where chaos leads to breakdown of adiabaticity as explained in the main text, while vertical dashed lines mark the location of the horn avoided crossings. The interaction parameter is $u = 0.2$. Here and in all subsequent figures we set ε=0.1 for the detuning. **(b)** The effective interaction parameter $u_{\rm eff}(x)$ for the same u. Additionally we plot the chaoticity measure t_s, see Fig.4 for its definition. **(c)** The adiabatic E[SP] energies for the same u. The followed state corresponds to the middle curve. **(d)** Emergence of the horn state. The E[SP] of the followed state is zoomed for $u = 0$ (dotted gray), $u = 0.1$ (dashed black), and u=0.101 (solid magenta).

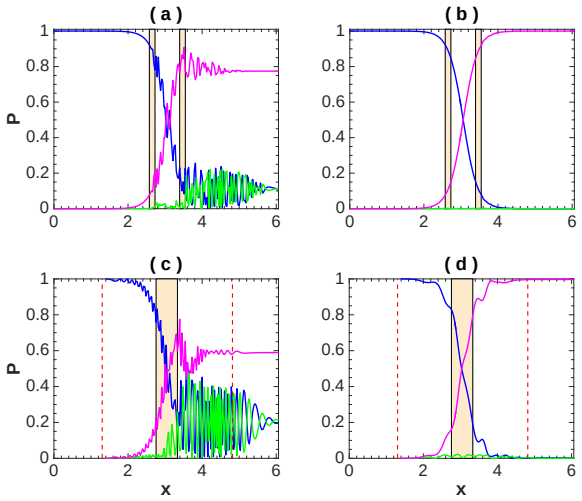

FIG. 2. (color online) The evolution of the site populations is plotted versus $x(t)$. The locations of the horn crossings (if exist) and of the chaotic intervals of Fig.1ac are indicated. **(a)** Failure of STIRAP in the absence of SP bifurcations: here $u = 0.8\varepsilon$ is *below* the critical value for obtaining the horn crossing. The sweep rate is $\dot{x}/K = 6 \times 10^{-5}$. **(b)** Recovery of adiabatic passage when the sweep rate is *increased* ($\dot{x}/K = 6 \times 10^{-4}$) during the marked chaotic intervals. **(c)** Failure of STIRAP for u=0.22, with initial conditions that bypasses the horn crossing: the process is launched at the adiabatic state *after* the avoided crossing. Sweep rate is $\dot{x}/K = 6 \times 10^{-3}$. **(d)** For the same interaction strength, efficiency is recovered due to faster sweep ($\dot{x}/K = 3 \times 10^{-2}$) during the chaotic interval.

where the dimensionless parameters are the interaction $u = NU/K$, the detuning $\varepsilon = \mathcal{E}/K$, and the couplings $g_{p,s} = \Omega_{p,s}/K$. We also define the effective nonlinearity $u_{\rm eff}(x) = u/(g_p^2(x) + g_s^2(x))^{1/2}$. The latter is largest at the beginning and at the end of the sweep, where the linear coupling terms are small, see Fig.1b.

Bifurcation diagram.– The x-dependent SPs studied in [30], satisfy $i\dot{\mathbf{a}} = \mu\mathbf{a}$ at fixed x, where μ is the chemical potential. For $u = 0$ there are three SPs, corresponding to the adiabatic eigenstates of linear STIRAP [6]. In the presence of interaction the SPs bifurcate if the effective interaction $u_{\rm eff}(x)$ is large enough, i.e. at early and late times, as shown in Fig.1c. For $u > \varepsilon$ the 'horn' avoided crossing appears [30], as illustrated in Fig.1d. As the nonlinearity (u) increases, more SPs emerge.

Irrelevance of bifurcations.– In the spirit of the two-mode energetic stability paradigms, the loss of adiabaticity in the nonlinear three-mode STIRAP scheme, was attributed to the appearance of the horn crossing [30]. However, a careful inspection of the nonlinear STIRAP process shows that the interaction-induced breakdown of adiabaticity goes beyond the bifurcation diagram analysis. In fact, as shown in Fig.2a, inefficient transfer in the adiabatic limit ($\dot{x} \to 0$) is obtained even for $u < \varepsilon$, where no horn crossing is present. Note that the population oscillations that indicate non-adiabaticity, are boosted only during the two marked narrow intervals in Fig.2a, for which the adiabatic bifuraction diagram exhibits no special nonlinear features. Moreover, as demonstrated in Fig.2c, while for $u > \varepsilon$ the horn crossing does appear in an early stage, adiabaticity breaks down even if the system is initiated *after* it. Here too, the growth of population oscillations does not correlate with the location of the avoided crossing or any other feature in the bifurcation diagram.

Another unique finding is the dependence of the transfer efficiency on the sweep rate. Strangely enough, the efficiency increases for *faster* sweep rates. In fact, as demonstrated in Fig.2b and Fig.2d, adiabaticity can be restored by speeding up the sweep process only during the well-defined marked intervals mentioned above. This prescription obviously has nothing to do with bifurcations of stationary solutions.

We thus conclude that the breakdown of adiabaticity in the quasi-static limit takes place irrespective of the bifurcation diagram. Below we establish that a different mechanism is responsible for this breakdown.

Passage through chaos.– In Fig.3, we show representative Poincare sections for several x values during the

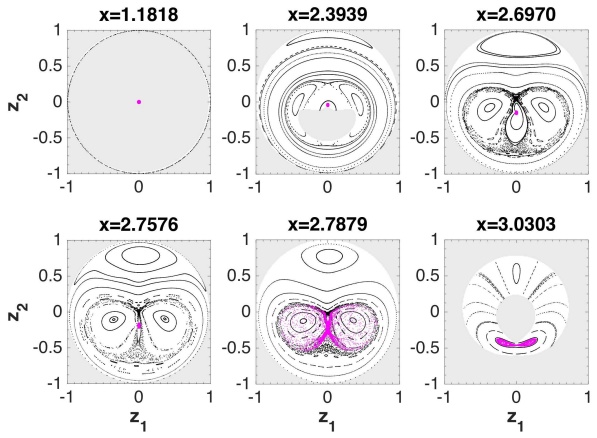

FIG. 3. (color online) Poincare sections for the frozen (time-independent) Hamiltonian for representative values of x. Here u=0.22. Each x-panel corresponds to the dynamics at the energy $E = E$[SP] of the followed-SP. The cross section of the trajectories is taken through the $n_2 = n_2$[SP] plane of the 3D energy surface. We use polar coordinates $z = (\varphi, r)$ where $\varphi = \varphi_1 - \varphi_3$ is the phase difference, and $r = (1 - (n/N))/2$ reflects the population imbalance $n = n_1 - n_3 \in [-N, N]$. Magenta dots correspond to a semiclassical cloud, initially localized around the followed-SP. Gray shading marks energetically forbidden regions. Note that these panels depict the adiabatic sequence up to the middle point $x \sim 3$. The Poincare sections at later times mirror the presented panels, and contain a second chaotic interval.

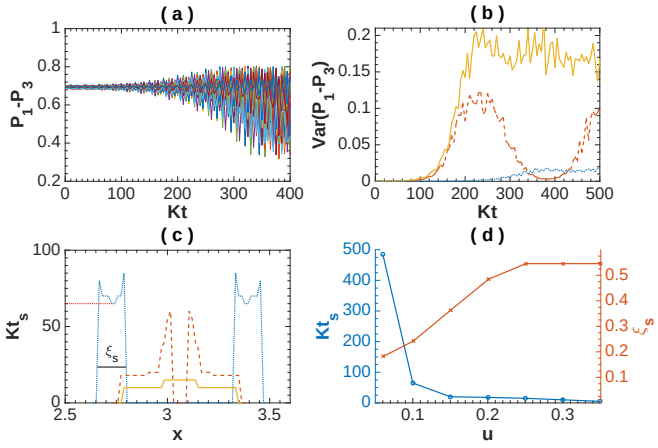

FIG. 4. (color online) Quasi-stationary spreading dynamics in the chaotic strip. **(a)** Time evolution of the population imbalance $P_1 - P_3$ of representative trajectories in the semiclassical cloud, for u=0.1 and fixed $x = 2.7273$. **(b)** The resulting variance growth of the initially localized cloud for $u = 0.1$ (dotted blue), 0.2 (dashed red), 0.3 (solid orange), with fixed x within the chaotic range. The spreading is ballistic with a stochastic component. The spreading time t_s to double the initial variance is numerically extracted. **(c)** The dependence of the spreading time t_s on x for $u = 0.1, 0.2, 0.3$ (line types same as in b). Outside of the chaotic intervals $t_s = 0$ means 'no spreading'. From here we find, for the given u, the chaotic interval width ξ_s. The associated limiting t_s is the minimal value within this chaotic interval. **(d)** The dependence of ξ_s ($\times$) and t_s ($\circ$) on the interaction u.

adiabatic passage. The Poincare sections are taken at the followed adiabatic energy $E = E$[SP]. Coordinates are chosen such that the radius corresponds to the population imbalance $n = n_1 - n_3$, and the azimuth corresponds to the relative phase $\varphi = \varphi_1 - \varphi_3$. It is important to clarify that the observed structures do not reflect the topography of the energy landscape, but correspond to various periodic orbits, invariant tori, and chaotic regions *on the same energy surface*. The plotted sections contain a single SP that supports the followed adiabatic eigenstate, while the other 'fixed-points' are in fact periodic orbits. In each section, we plot the evolution of a cloud that is launched around the followed-SP.

The sequence of Poincare sections clearly reveals the mechanism that is responsible for the breakdown of the STIRAP efficiency. At early times (Fig.3, $x = 1.1818$) the two coupling pulses are too weak to induce transitions between the trimer sites and the dynamics is interaction-dominated. The evolution is restricted to self-trapped trajectories, and the followed SP is *energetically stable*: it is surrounded by an energetically forbidden region (gray). As the coupling increases this forbidden region disappears and an intermediate non-linear resonance shows up as a 'belt' in the Poincare section. The presence of this belt structure becomes prominent as x is increased (Fig. 3, $x = 2.3939$). At larger x, the belt expands, and a chaotic strip is formed along its border. The enclosed 'island', which contains the followed-SP, shrinks down (Fig.3, $x = 2.6970$) until the SP hits the chaotic strip ($x = 2.7576$). The intervals during which adiabaticity breaks down correspond to the embedding of the followed-SP in the chaotic strip, resulting in the quasi-stochastic spreading of the initially localized distribution over the chaotic region (Fig.3, $x = 2.7879$). The entire progression takes place on a single 3D energy surface, and has no trace in the adiabatic energy diagram. Thus the breakdown of STIRAP efficiency is not due to the destruction of *energetic stability*, but rather due to the loss of *dynamical stability*.

Adiabaticity threshold.– The *passage through chaos mechanism* also explains why the speed-up of the sweep during the chaotic intervals can restore the STIRAP efficiency. The spreading during the chaotic intervals (see Fig.4) is characterized by a typical spreading onset time t_s followed by ballistic expansion throughout the stochastic strip. The draining of the SP region can be practically avoided if the chaotic interval ξ_s is traversed on a time scale which is short compared with t_s. This leads to the deduction of a *lower adiabaticity threshold*. Combining with the standard adiabaticity condition we deduce that high STIRAP efficiency is maintained for

$$\frac{\xi_s}{t_s} \;<\; \dot{x} \;<\; \frac{1}{3\pi} K \qquad (3)$$

The upper limit condition is required for 96% efficiency [6] and ensures small probability for non-adiabatic transitions in the transverse (energy) direction. If $\dot{x}$ is constant throughout the evolution, the adiabaticity threshold condition translates into $\tau < t_s/x_s$ for the sweep time. For larger u, the ξ_s range becomes larger, while t_s becomes smaller (see Fig.4d). Consequently the adiabaticity threshold is monotonically increasing as a function of u.

Horn vs Belt resonance.– The horn avoided crossing [30] can be regarded as a 1:1 resonance. It is born provided $u > \varepsilon$ such that the condition $Un_1 = \mathcal{E}$ can be satisfied. We realize that there is also a nonlinear 2:1 resonance that manifests itself if $u > \varepsilon/2$, and shows up in the Poincare section as a belt that consist of two islands. This belt is born far away from the followed SP, but nevertheless it can choke the SP in a later stage.

We would like to clarify that weak non-adiabatic effects due to horn resonance can be detected as well, but for repulsive interactions ($u > 0$), as discussed above, they are overwhelmed by the passage-through-chaos mechanism. In contrast, for an attractive interaction ($u < 0$) the situation is quite different. The Poincare sections in this case (not displayed) show that the SP does not go through the chaotic strip of the non-linear belt. Consequently, in the latter case, the passage-through-chaos mechanism becomes irrelevant, and the failure of STIRAP is purely due to the horn crossing effect.

STIRAP efficiency.– Our results are summarized in Fig. 5, showing the STIRAP efficiency as a function of the interaction parameter u for several values of $\dot{x}$, as well as the complimentary dependence on $\dot{x}$ at fixed u. The shrinking of the u region where STIRAP efficiency is ∼100% as $\dot{x}$ is decreased, reflects the breakdown of adiabaticity due to the passage-through-chaos mechanism. In the adiabatic regime (panels c-d), the range of ∼100% efficiency is restricted by the *chaoticity threshold* ($|u| < |\varepsilon|/2$) below which no stochastic strips are formed. We note that a similar plot in Ref. [30] corresponds to an intermediate value of $\dot{x}$, hence it does not represent the adiabatic regime.

Looking at the dependence of the efficiency on the sweep rate (right panels of Fig. 5), we see that below the chaoticity limit (panel e) there is no breakdown in the slow sweep limit, and the efficiency is monotonically decreasing with the rate, just as in the linear case. Once chaos sets in (panels f-h), high efficiency can still be maintained if condition Eq.(3) is satisfied. As u is further increased, the high efficiency range between the 'slow' and 'fast' sweep boundaries shrinks, until the two inequlities of Eq.(3) can not be satsified simultaneously (panel h).

The transfer probability P_3 can be written as a sum $P_{\rm surv} + P_{\rm scat}$, where $P_{\rm surv}$ is the probability for survival in the SP region, while $P_{\rm scat}$ the scattered component. The former can be estimated as follows: The spreading trajectories in the stochastic region have frequencies

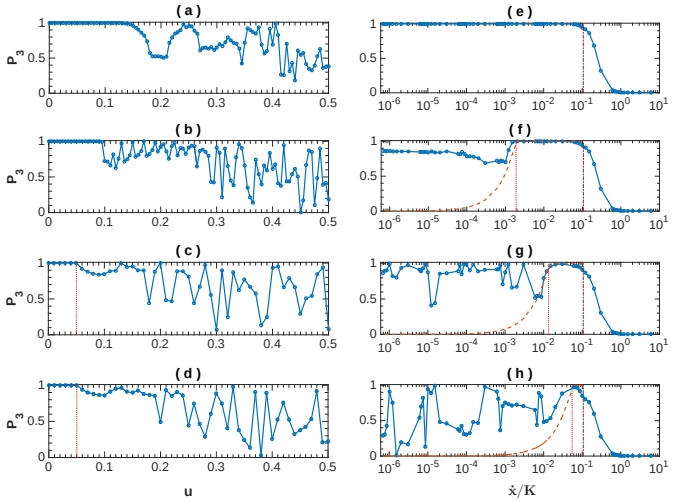

FIG. 5. (color online) STIRAP efficiency. P_3 is the fraction of the population that is transferred to the target state at the end of the nonlinear sweep process. In the left panels it is shown as a function of u for $\dot{x}/K$ values of (a) $6{\times}10^{-3}$, (b) $6{\times}10^{-4}$, (c) $6{\times}10^{-6}$, (d) $6{\times}10^{-7}$. The vertical lines in the lower left panels mark the chaoticity threshold $u = \varepsilon/2$. The panels on the right present the same efficiency as a function of the sweep rate $\dot{x}$ for u values of (e) 0.05, (f) 0.1, (g) 0.2, (h) 0.3. Vertical lines border the sweep rate range determined by the adiabaticity condition Eq.(3). The estimated SP survival probability Eq.(4) is plotted as orange dashed line.

$\omega \in [0, 1/t_s]$ with roughly uniform distribution. Trajectories that survive in the SP region satisfy $\omega \times (\xi_s/\dot{x}) < 1$, hence their fraction is

$$P_{\rm surv} \quad = \quad \min\{(t_s/\xi_s)\dot{x},\ 1\} \qquad (4)$$

This estimate can serve as a lower bound for the STIRAP efficiency as illustrated in Fig.4 panels f-h.

Conclusions.– We have found that the breakdown of adiabaticity in three-mode adiabatic passage schemes, such as STIRAP, is governed by far more intricate physics than that of the nonlinear Landau-Zener paradigm. The latter relies entirely on *energetic stability*, which is endangered by bifurcations of the followed-SP. By contrast, the failure of adiabatic passage in non-integrable systems is related to *dynamical instability* on a single multi-dimensional energy surface that contains both quasi-integrable and chaotic regions. One puzzling consequence of this observation is the possibility to improve adiabatic-passage efficiency by faster variation of the control parameters. Future work would focus on the quantum aspects of STIRAP in interacting many-body systems and the implications for linear response theory.

[1] L. D. Landau, Phys. Z. Sowjetunion **2**, 46 (1932).
[2] C. Zener, Proc. R. Soc. London, ser. A **137**, 696 (1932).
[3] E. C. G. Stuckelberg, Helv. Phys. Acta **5**, 369 (1932).
[4] E. Majorana, Nuovo Cimento **9**, 45 (1932).
[5] Gaubatz, U., P. Rudecki, S. Schiemann, and K. Bergmann, J. Chem. Phys. **92**, 5363 (1990).
[6] N. V. Vitanov, A. A. Rangelov, B. W. Shore, and K. Bergmann, Rev. Mod. Phys. **89**, 015006 (2017).
[7] B. M. Zobay and B. M. Garraway, Phys. Rev. A **61**, 033603 (2000).
[8] B. Wu and Q. Niu, Phys. Rev. A **61**, 023402 (2000).
[9] J. Liu, L.-B. Fu, B.-Yi. Ou, S.-G. Chen, D.-I. Choi, B. Wu, and Q. Niu Phys. Rev. A 66, 023404 (2002)
[10] J. Liu, B. Wu and Q. Niu, Phys. Rev. Lett. **90**, 170404 (2003).
[11] D. Witthaut, E. M. Graefe, and H. J. Korsch, Phys. Rev. A **73**, 063609 (2006)
[12] D. Witthaut, F. Trimborn, V. Kegel, and H. J. Korsch, Phys. Rev. A 83, 013609 (2011).
[13] A. M. Ishkhanyan, Europhys. Lett. **90**, 30007 (2010).
[14] J. R. Anglin, Phys. Rev. A **67**, 051601(R) (2003).
[15] A. Altland and V. Gurarie Phys. Rev. Lett. **100**, 063602 (2008).
[16] F Trimborn, D Witthaut, V Kegel, and H J Korsch, New J. Phys. **12**, 053010 (2010).
[17] K. Smith-Mannschott, M. Chuchem, M.Hiller, T. Kottos, and D. Cohen Phys. Rev. Lett. **102**, 230401 (2009).
[18] Y.-A. Chen, S. D. Huber, S. Trotzky, I. Bloch, and E. Altman, Nature Physics **7**, 61 (2011).
[19] S. F. Caballero-Benitez and R. Paredes, Phys. Rev. A 85, 023605 (2013).
[20] J. Javanainen and M. Mackie Phys. Rev. A **59**, R3186(R) (1999).
[21] V. A. Yurovsky, A. ben-reuven, P. Julienne, and C. J. Williams, Phys. Rev. A **62**, 043605 (2000).
[22] D. J. Heinzen, Roahn Wynar, P. D. Drummond, and K. V. Kheruntsyan, Phys. Rev. Lett. **84**, 5029 (2000).
[23] A. Ishkhanyan, M. Mackie, A. Carmichael, P. L. Gould, and J. Javanainen, Phys. Rev. A 69, 043612 (2004).
[24] E. Altman and A. Vishwanath, Phys. Rev. Lett. 95, 110404 (2005).
[25] E. Pazy, I. Tikhonenkov, Y. B. Band, M. Fleischhauer, and A. Vardi, Phys. Rev. Lett. **95**, 170403 (2005).
[26] I. Tikhonenkov, E. Pazy, Y. Band, M. Fleischhauer, and A. Vardi, Phys. Rev. A 73 043605 (2006).
[27] J. Liu, B. Liu, and L. B. Fu, Phys. Rev. A **78**, 013618 (2008).
[28] J. Liu, L.-B. Fu, B. Liu, and B. Wu, New J. Phys. 10 123018 (2008).
[29] G. Arwas, A. Vardi, and D. Cohen, Sci. Rep. **5**, 13433 (2015).
[30] E. M. Graefe, H. J. Korsch, and D. Witthaut, Phys. Rev. A **73**, 013617 (2006).
[31] M. Rab, J. H. Cole, N. G. Parker, A. D. Greentree, L. C. L. Hollenberg, and A. M. Martin, Phys. Rev. A **77**, 061602(R) (2008).
[32] C. J. Bradly, M. Rab, A. D. Greentree, and A. M. Martin, Phys. Rev. A 85, 053609 (2012).
[33] J. Polo, A. Benseny, Th. Busch, V. Ahufinger, and J. Mompart, New J. Phys. **18**, 015010 (2016).
[34] M. Dupont-Nivet, M. Casiulis, T. Laudat, C. I. Westbrook, and S. Schwartz, Phys. Rev. A 91, 053420 (2015).
[35] J. C. Eilbeck, G. P. Tsironis, and S. K. Turitsyn, Phys. Scr. **52**, 386 (1995).
[36] D. Hennig, H. Gabriel, M.F. Jorgensen, P.L. Christiansen, and C.B. Clausen, Phys. Rev. E **51**, 2870 (1995).
[37] R. Franzosi, V. Penna, Phys. Rev. E **67**, 046227 (2003).
[38] S. Flach and V. Fleurov, J. Phys.: Condens. Matter **9**, 7039 (1997).
[39] K. Nemoto, C.A. Holmes, G.J. Milburn, and W.J. Munro, Phys. Rev. A **63**, 013604 (2000).
[40] R. Franzosi and V. Penna, Phys. Rev. A **65**, 013601 (2002).
[41] M. Hiller, T. Kottos, and T. Geisel, Phys. Rev. A **73**, 061604(R) (2006).
[42] I. Tikhonenkov, A. Vardi, J. R. Anglin, and D. Cohen, Phys. Rev. Lett. **110**, 050401 (2013).